Optics Letters

UV 30 fs laser pulse generation using a multi-pass cell

Victor Hariton,[1,*] Yujiao Jiang,[1] Arthur Schönberg,[1] Marcus Seidel,[1,2,3] Marek Wieland,[4] Mark J. Prandolini,[4,5] Ingmar Hartl,[1] Markus Drescher,[4] and Christoph M. Heyl[1,2,3]

[1]Deutsches Elektronen-Synchrotron DESY, Notkestraße 85, 22607 Hamburg, Germany
[2]Helmholtz Institute Jena, Jena, Germany
[3]GSI Helmholtzzentrum für Schwerionenforschung GmbH, Darmstadt, Germany
[4]Universität Hamburg, Institut für Experimentalphysik, Luruper Chaussee 149, 22761 Hamburg, Germany
[5]Class 5 Photonics, Notkestraße 85, 22607 Hamburg, Germany
*victor.hariton@desy.de

Received 23 April 2024; revised 7 June 2024; accepted 10 June 2024; posted 11 June 2024; published 27 June 2024

Ultrashort ultraviolet (UV) pulses are pivotal for resolving ultrafast electron dynamics. However, their efficient generation is strongly impeded by material dispersion and two-photon absorption, in particular, if pulse durations around a few tens of femtoseconds or below are targeted. Here, we present a new (to our knowledge) approach to ultrashort UV pulse generation: using the fourth-harmonic generation output of a commercial ytterbium laser system delivering 220 fs UV pulses, we implement a multi-pass cell (MPC) providing 5.6 µJ pulses at 256 nm, compressed to 30.5 fs. Our results set a short-wavelength record for MPC post-compression while offering attractive options to navigate the trade-off between upconversion efficiency and acceptance bandwidth for UV pulse production.

https://doi.org/10.1364/OL.527988

Ultrafast laser pulses are indispensable in many scientific and commercial areas. In particular, the ultraviolet (UV) spectral range plays an increasingly important role with applications in nonlinear optics and time-resolved spectroscopy [1]. In addition, in recent years, several free-electron laser (FEL) facilities have explored the concept of seeding the FEL process by UV laser pulses to increase power stability and spectral brightness [2]. Researchers have employed various methods for ultrashort UV pulse generation. These are typically based on doubling, tripling, or quadrupling the frequency of infrared (IR) lasers in nonlinear crystals, which has enabled the generation of sub-20 fs UV pulses [3,4]. Advanced techniques have taken this further, achieving sub-10 fs pulses [5]. However, these methods often suffer from two-photon absorption, phase matching bandwidth limitations, group delay mismatch, spatial walk-off effects, and consequently low conversion efficiency as well as poor beam quality for ultrashort pulses. Such schemes are typically limited to sub-10% conversion efficiency for pulse durations below 100 fs [6,7]. Another approach is harmonic frequency conversion of longer laser pulses, followed by spectral broadening using nonlinear phase modulation of UV pulses in solid and gaseous media and subsequent compression. This method has been used to compress frequency upconverted Ti:sapphire laser pulses at 266 nm down to 23 fs [8] and in a separate experiment down to 8 fs [9]. In addition, 100-fs pulses from a KrF excimer laser (emitting at 248 nm) have been post-compressed, reaching sub-20-fs pulses at 20 µJ pulse energy [10]. An alternative scheme employs resonant dispersive wave (RDW) emission in gas-filled hollow-core fibers (HCFs), transferring the energy from the soliton, yielding tunable microjoule-level (1–16 µJ) pulses with sub-10-fs pulse duration [11]. Furthermore, a recent report demonstrated 6 fs, 11 µJ UV pulse generation from Cross-Phase Modulation (XPM) of a Ti:sapphire laser pulse and its third harmonic [12].

In this study we explore the potential of multi-pass cell (MPC)-based spectral broadening and compression for the generation of ultrashort UV pulses. MPCs have shown remarkable success, currently operating predominantly in the near infrared (NIR) spectral region. They enable compression factors exceeding 30 in a single stage with excellent efficiencies beyond 95% [13,14]. MPC-based post-compression systems enable efficient few-cycle pulse production with high spatial beam quality [15–17], reaching high pulse energies exceeding 100 mJ and supporting high average powers reaching the kW range [13,18]. At shorter wavelengths, gas-based MPCs have been used to efficiently compress 250-fs pulses down to sub-20-fs, with efficiencies exceeding 85% in the green (515 nm) spectral region [19,20], setting the current short-wavelength record for MPC post-compression. Extending MPC methods toward even shorter wavelength opens opportunities for efficient ultrashort UV pulse generation. However, this development direction imposes multiple challenges set by mirror coatings, which compared to their near infrared counterparts [21], suffer from two-photon absorption which is more pronounced at shorter wavelengths as well as at higher dispersion.

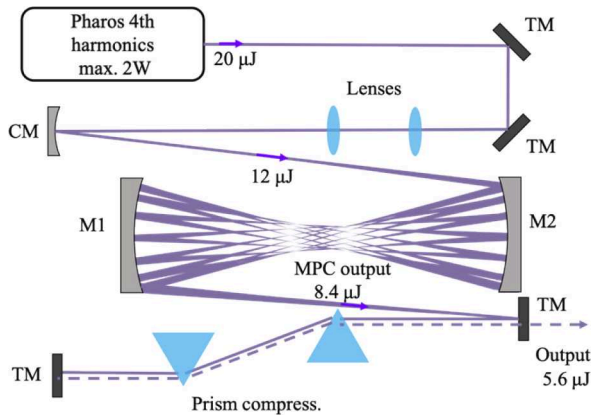

Fig. 1. Layout of the broadening setup using a multi-pass configuration. The fourth-harmonic module of the laser (Light Conversion Pharos) produces pulses at 256 nm. Air is used as the nonlinear medium for spectral broadening. A prism compressor is used to remove the chirp.

Table 1. Parameters Used for Spectral Broadening in Gaseous Nonlinear Media[a]

Multi-Pass Cell Parameters	
Cell mirror ROCs (mm)	−500; −500
Distance between mirrors (mm)	677
Number of round trips	13
Spot waist ($1/e^2$) in focus (μm)	140
B_{int} per pass (rad)	~1.07
Fluence on mirror (mJ/cm^2)	13
Peak intensity on mirror (GW/cm^2)	54
Pressure (bar)	1
n_{2R} (m^2/W)	$8.7 \cdot 10^{-23}$ [25]
n_{2i} (m^2/W)	$1.37 \cdot 10^{-23}$ [27]
Input duration (fs)	220
Input pulse energy (μJ)	12
Peak intensity in focus (TW/cm^2)	3.3
Output FTL duration (fs)	27
Output pulse energy (μJ)	5.6

[a]Spatial beam properties were calculated assuming linear mode-matching.

Here we report, for the first time to our knowledge, spectral broadening in MPCs in the UV spectral region and demonstrate pulse compression from 220 to 30 fs at 256 nm. Using a simple MPC setup employing ambient air as a nonlinear medium, we generate 5.6 μJ UV pulses with excellent spatial beam quality ($M^2 < 1.2$). Our results open up opportunities for efficient ultrashort UV pulse generation and extend a very versatile pulse compression scheme to a new spectral region.

For our experiments, we employ a commercial Yb-based laser system (Light Conversion Pharos) that delivers a frequency-quadrupled output directly at 256 nm. The maximum available pulse energy in the UV is 20 μJ at a pulse duration of 220 fs, corresponding to an average power of 2 W at 100 kHz repetition rate. The optical setup is shown in Fig. 1, consisting of a mode-matching unit and an MPC followed by a prism compressor. The MPC consists of two concave dielectric coated mirrors, each 50 mm in diameter with 500 mm (M_1, M_2) radii of curvature (ROC), and ambient air as the nonlinear medium. The dielectric mirrors support a spectral range between 245 and 275 nm at >99% reflectivity. The MPC mirror spacing was set to 677 mm, resulting in 26 passes through air. The corresponding calculated Gaussian eigenmode radius for a wavelength of 256 nm is $w_0 = 140$ μm at the focus with $w_{1,2} = 240$ μm beam radii at the surface of the $M_{1,2}$ mirrors. A summary of the experimental parameters is provided in Table 1. A lens telescope followed by a ROC = 0.5 m concave mirror matches the input beam to the eigenmode of the MPC. The input/output coupling within the cell is managed by a scraper mirror. Losses from the telescope optics and the transport mirrors allow a maximum of 12 μJ at the MPC input.

The chosen cell geometry allows a suitable balance between achieving a reasonable nonlinear phase shift in the medium, keeping the fluence at the mirror surfaces low while avoiding ionization. The calculated B-integral per single focal passage is $B_{int}^{tot} \sim 1$ rad. The ~99% reflectivity of the dielectric UV mirrors is low compared to standard NIR high reflectance (HR) mirrors. Consequently, only 13 round trips were chosen to reach 70% total transmission of the spectral broadening setup. In addition, the linear dispersion of the nonlinear media is higher in the UV, and dispersion management via chirped mirrors to prevent excessive temporal pulse broadening is challenging in this spectral region. Group delay dispersion (GDD) curves typically exhibit large oscillations [21], and the reflectivity of dispersive optics is significantly lower (<95%) in the UV compared to that in the NIR, making them impractical for multi-pass configurations. These limitations imply that the use of HR mirrors, short path lengths, inside the medium and a low number of reflections are preferable. Similar approaches have been implemented in the visible for the broadening of 515 nm laser pulses in MPC configurations [18,19]. Highly reflective non-dispersive mirrors can be fabricated with a high damage threshold (~0.5 J/cm^2) in the UV range supporting a stable and reliable long-term operation. Therefore, spectral broadening setups with low dispersion in the medium are desirable. Nitrogen, which is the main component of ambient air (77%), has a group velocity dispersion (GVD), at 1 bar, of 95.1 fs^2/m [22]. The induced dispersion in the UV is approximately six times higher than in the NIR.

The measured dependence of the MPC output spectrum on the input energy is shown in Fig. 2(a)). Pulse energy scaling up to 12 μJ input energy is shown together with corresponding simulations for selected energies (5.7, 7.7, 9.8, and 12 μJ), Fig. 2(b)). We perform a series of simulations using a computational model, which uses a three-dimensional (2D + 1) approach to solve the Unidirectional Pulse Propagation Equation (UPPE)

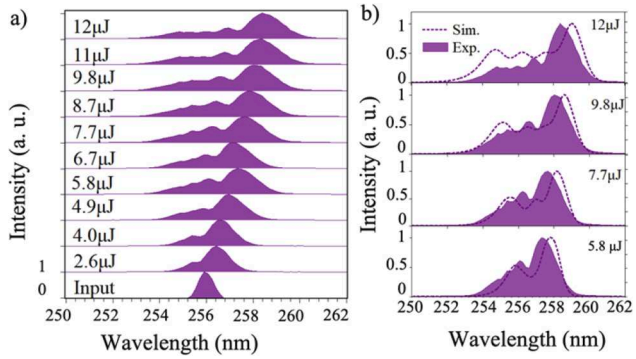

Fig. 2. (a) Measured evolution of the MPC output spectra depending on input energy. (b) Experimental data sets displayed together with the corresponding simulations for selected energies (5.8, 7.7, 9.8, and 12 μJ).

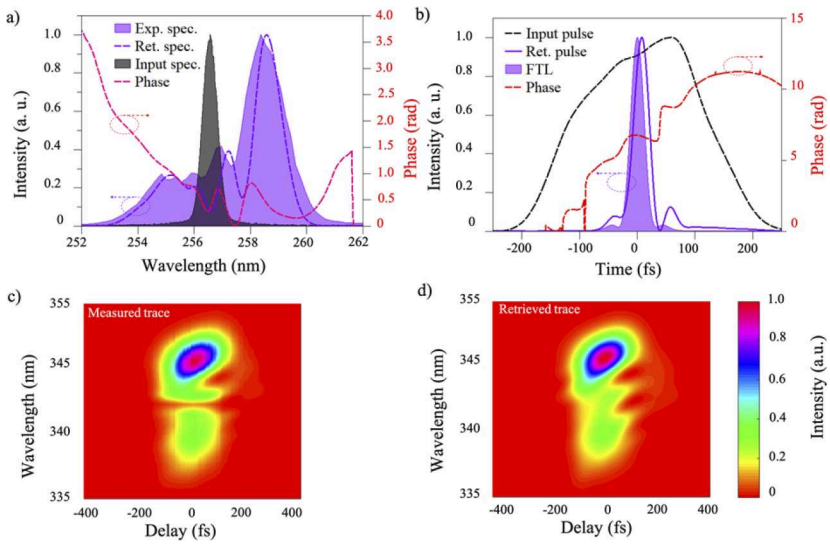

Fig. 3. (a) Measured (violet shaded area) and FROG-retrieved (violet dashed line) output spectrum and spectral phase (red dashed line) at an input energy of 12 µJ displayed together with the spectrum of the MPC input pulse (gray shaded area). (b) FROG-retrieved temporal profile (violet solid line), temporal phase profile (red dashed line), and FTL reference (shaded area) together with the retrieved input pulse profile (black dashed line). The retrieved pulse duration is 30.5 fs with an FTL of 27 fs. (c) Measured and (d) reconstructed FROG traces. The FROG error is 7×10^{-3} on a 256×256 grid.

[23]. The simulation code incorporates various laser pulse propagation phenomena, including linear effects such as dispersion and diffraction, as well as nonlinear effects such as the optical Kerr effect, self-steepening, and both instantaneous and delayed Raman effects. In order to model the Raman–Kerr interaction, we use the damped harmonic oscillator model [24], which parametrizes the interaction of the laser field with the rotational states of a molecular gas within a single harmonic oscillator. This simplified model requires the period of the oscillation t_1, the damping time t_2, the Raman–Kerr fraction f_R, and the non-instantaneous fraction of the nonlinear refractive index of air n_{2R}. The values for 1 bar of air at 220 fs pulse duration and 256 nm are given by $t_1 = 62.5$ fs, $t_2 = 71.4$ fs, $f_R = 0.7$ [24]. The value for $n_{2R} = 5.4 \times 10^{-23}$ m^2/W (at 800 nm [25]) is scaled to 256 nm according to the wavelength scaling equation of the nonlinear refractive index provided in [26], which results in n_{2R} (256 nm) $= 8.72 \times 10^{-23}$ m^2/W. Analogously, the instantaneous nonlinear refractive index is scaled to n_{2i} (256 nm) $= 1.37 \times 10^{-23}$ m^2/W [27]. The numerical simulations agree reasonably well with the experimental results at each energy step. We attribute the remaining discrepancies to model simplifications (only nitrogen is considered as nonlinear medium) and inaccuracies of the Raman constants. At the highest energy, the spectrum extends from 253 to 259 nm, corresponding to a Fourier transform limit (FTL) of 27 fs. The central wavelength is shifted toward the red side. We attribute this asymmetry to the Raman effect and the asymmetric pulse shape of the input pulse (displayed in Fig. 3(b)). The harmonic unit of the Pharos system produces pulses with a slightly asymmetric temporal shape. This asymmetry will result in broadening with unevenly distributed frequencies around the center [28]. In the presented case, a combination of this effect and the Raman effect occurs, resulting in the measured output spectrum.

The asymmetric spectral shape does not affect the compressibility. The broadened pulses were compressed using a prism pair compressor. The prisms are made of CaF_2 and placed at

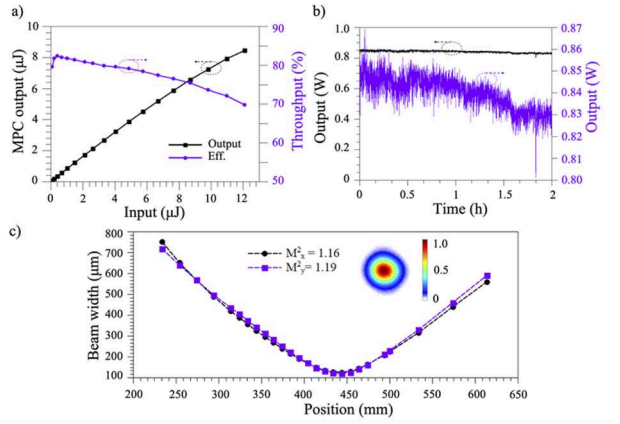

Fig. 4. (a) Measured MPC output pulse energy, before compression, as a function of input energy displayed together with the overall efficiency of the MPC. (b) Measured power stability (zoom-in scale on the right vertical axis). (c) M^2 measurements at 256 nm. The inset displays the measured beam profile near the focus.

a distance of 280 mm. A maximum of 5.6 µJ is measured after the compressor. The attenuated compressed pulses are sent to a home-built cross correlation frequency-resolved optical gating (X-FROG) setup described in [29] for characterization. A measured pulse duration of 30.5 fs was retrieved as shown in Fig. 3(b)). The recorded and retrieved FROG traces are shown in Figs. 3(c)) and 3(d)), respectively.

The measured output energy and the corresponding efficiency are plotted in Fig. 4(a)). A decrease in efficiency is observed as the fluence on the mirrors is increased. We attribute this effect to a decreased mirror reflectivity toward the edges of the mirror bandwidth as well as to an increased nonlinear lensing at higher peak power affecting mode-matching. A power stability measurement (Fig. 4(b)) was conducted over 2 h of

continuous operation. The system maintained consistent performance throughout the measurement period, with fluctuations comparable to those of the source. In addition, the beam quality was measured using a commercial M^2 meter (CINOGY Technologies: CinSquare M^2 Tool). An M^2 of less than 1.2 was measured for both axes, indicating no beam quality degradation comparable to the input beam, which is also 1.2 as defined by the manufacturer.

Our approach for ultrashort UV pulse generation utilizing the fourth-harmonic generation of long NIR laser pulses followed by post-compression relaxes the constraints on the SHG crystal parameters. While previous studies have achieved long-term operation using high quality crystals for ultrashort UV pulse generation via frequency upconversion, additional techniques such as crystal rotation and beam spot shifting have been required [30]. The use of long pulses for frequency upconversion together with reflective optics offers a route to mitigate this effect. Note that chirped mirrors can be used to replace the prism compressor in order to avoid transmissive optical elements. In comparison with other UV pulse generation methods, another important characteristic to consider is wavelength tunability. In comparison to frequency-upconverted ultrafast sources employing parametric amplifiers, our approach relying on a post-compressed Ytterbium laser is more efficient and provides better beam properties. On the other hand, parametric amplifiers can be tuned more easily. The MPC approach would require different mirror sets if combined with efficient, tunable lasers. Our method also promises scalability to higher average power. Additional up-scaling of the input energy is prospectively possible by using larger ROC mirrors and reduced gas pressure [31]. Shorter pulse durations could be attained by increasing the number of round trips and utilizing gases with higher nonlinearity, such as Nitrous oxide (N_2O), which allows for greater B-integral accumulation per pass.

In summary, this letter reports the first spectral broadening and post-compression experiments with MPCs in the UV spectral range. The results show the adaptability of MPCs to extended spectral regions while offering a new route for efficient ultrashort UV pulse production. Our method relies heavily on cell geometries with a minimized material interaction length and dispersion. These results demonstrate an overall conversion efficiency exceeding 4.5% from the infrared drive laser to the UV pulses after compression, which is comparable to records reached with alternative approaches [7,8]. However, direct improvements can prospectively be achieved by increasing the conversion efficiency of the fourth-harmonic unit, currently at 10% level, by using longer IR pulses and by optimizing the compression setup. The compressed pulses generated by this setup lead to a 7-fold reduction in pulse duration while maintaining high beam quality. Our results suggest efficient up-scaling options to higher average and peak powers.

Acknowledgment. We acknowledge Deutsches Elektronen-Synchrotron DESY (Hamburg, Germany), the Helmholtz Institute Jena (Jena, Germany), and members of the Helmholtz Association HGF for support and/or the provision of experimental facilities.

Disclosures. The authors declare no conflicts of interest.

Data availability. Data available upon reasonable request from the authors.

REFERENCES

1. M. Maiuri, M. Garavelli, and G. Cerullo, J. Am. Chem. Soc. **142**, 3 (2020).
2. N. Huang, H. Deng, B. Liu, *et al.*, The Innovation **2**, 100097 (2021).
3. N. Krebs, R. A. Probst, and E. Riedle, Opt. Express **18**, 6164 (2010).
4. C. Homann, P. T. Lang, and E. Riedle, J. Opt. Soc. Am. B **29**, 2765 (2012).
5. P. Baum, S. Lochbrunner, and E. Riedle, Appl. Phys. B **79**, 1027 (2004).
6. C.-L. Chang, P. Krogen, H. Liang, *et al.*, Opt. Lett. **40**, 665 (2015).
7. K. Liu, H. Li, S. Qu, *et al.*, Opt. Express **28**, 18360 (2020).
8. F. Noack, O. Steinkellner, P. Tzankov, *et al.*, Opt. Express **13**, 2467 (2005).
9. C. G. Durfee, S. Backus, H. C. Kapteyn, *et al.*, Opt. Lett. **24**, 697 (1999).
10. J.-H. Klein-Wiele, T. Nagy, and P. Simon, Appl. Phys. B **82**, 567 (2006).
11. J. J. C. Travers, T. F. Grigorova, C. Brahms, *et al.*, Nat. Photonics **13**, 547 (2019).
12. Y. Jiang, J. P. Messerschmidt, F. Scheiba, *et al.*, Optica **11**, 291 (2024).
13. T. Nagy, P. Simon, and L. Veisz, Adv. Phys.: X **6**, 1845795 (2021).
14. A. Viotti, M. Seidel, E. Escoto, *et al.*, Optica **9**, 197 (2022).
15. M. Müller, J. Buldt, H. Stark, *et al.*, Opt. Lett. **46**, 2678 (2021).
16. S. Goncharov, K. Fritsch, and O. Pronin, Opt. Lett. **48**, 147 (2023).
17. S. Rajhans, E. Escoto, N. Khodakovskiy, *et al.*, Opt. Lett. **48**, 4753 (2023).
18. M. Kaumanns, D. Kormin, T. Nubbemeyer, *et al.*, Opt. Lett. **46**, 929 (2021).
19. V. Hariton, A. B. Wahid, G. Figueira, *et al.*, Opt. Lett. **47**, 1246 (2022).
20. M. Karst, P. Pfaller, R. Klas, *et al.*, Opt. Lett. **48**, 1300 (2023).
21. P. V. Pervak, O. Razskazovskaya, I. B. Angelov, *et al.*, Adv. Opt. Technol. **3**, 55 (2014).
22. U. Griesmann and J. H. Burnett, Opt. Lett. **24**, 1699 (1999).
23. J. Andreasen and M. Kolesik, Phys. Rev. E **86**, 036706 (2012).
24. D. Langevin, J. M. Brown, M. B. Gaarde, *et al.*, Phys. Rev. A **99**, 063418 (2019).
25. E. T. J. Nibbering, G. Grillon, M. A. Franco, *et al.*, J. Opt. Soc. Am. B **14**, 650 (1997).
26. C. Bree, A. Demircan, and G. Steinmeyer, IEEE J. Quantum Electron. **46**, 433 (2010).
27. S. Zahedpour, J. K. Wahlstrand, and H. M. Milchberg, Opt. Lett. **40**, 5794 (2015).
28. P. Balla, H. Tünnermann, S. H. Salman, *et al.*, Nat. Photonics **17**, 187 (2023).
29. M. Seidel, X. Xiao, S. A. Hussain, *et al.*, Sci. Adv. **4**, 1 (2018).
30. Y. Orii, K. Kohno, H. Tanaka, *et al.*, Opt. Express **30**, 11797 (2022).
31. C. M. Heyl, M. Seidel, E. Escoto, *et al.*, J. Phys. Photonics **4**, 014002 (2022).